# Computational modeling of cancer cell metabolism along the catabolic-anabolic axes

Javier Villela-Castrejon, Herbert Levine, Benny A. Kaipparettu, José N. Onuchic, Jason T. George, Dongya Jia

**Supplementary Information**

**Supplementary Figure 1**

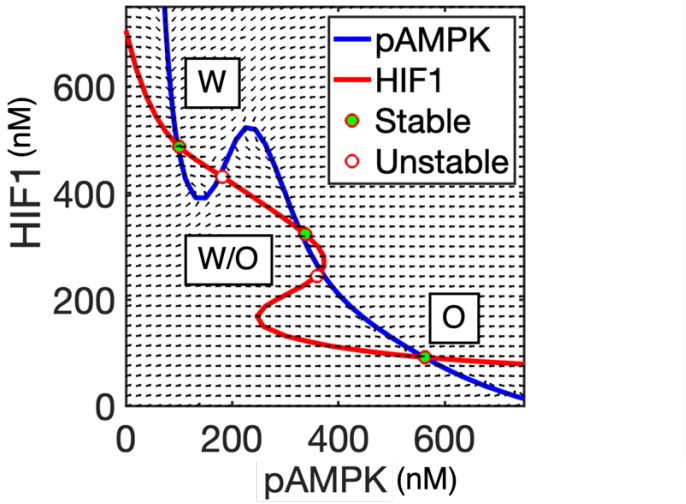


**Supplementary Figure 1: The nullclines and steady states** in the phase space of AMPK and HIF-1 when Myc = 1200 μM. The red line represents the nullcline where the rate of change of HIF-1 (*dH/dt*) is zero, and the blue line represents the nullcline where the rate of change of AMPK (*dA/dt*) is zero. Solid dots represent stable steady states while hollow dots represent unstable steady states. Each stable state is associated with a metabolic phenotype. With a low MYC expression, cells can acquire the Warburg phenotype, referred to as the state "W", an OXPHOS phenotype, referred to as the state "O", and a hybrid phenotype with intermediate activities of AMPK and HIF-1 called the state "W/O".

**Supplementary Figure 2**

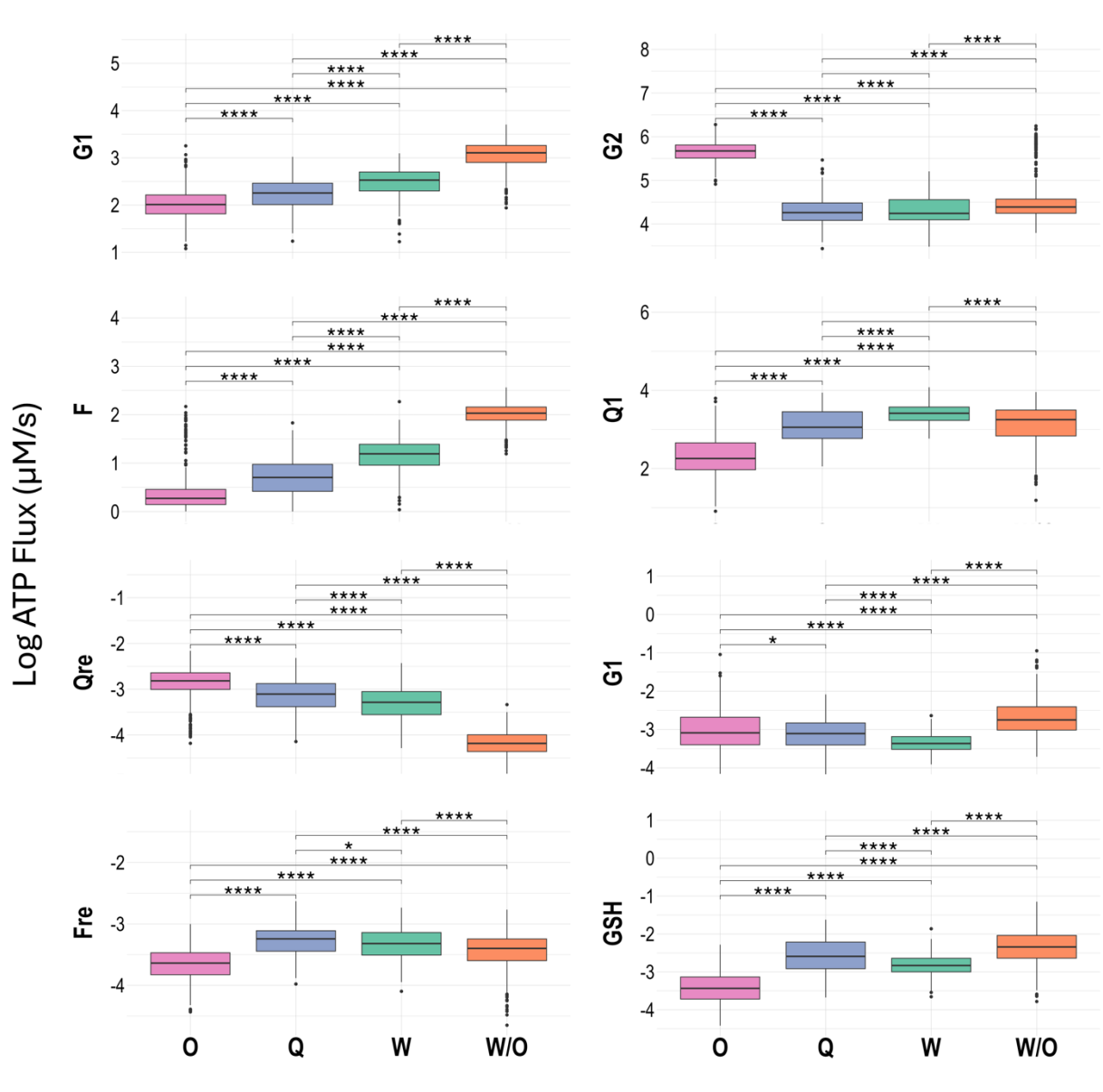


**Supplementary Figure 2: Log ATP flux of different metabolic pathways for the "O", "W/O", "W", and "Q" states.** Box plots summarizing and illustrating the differences in the log ATP flux of various metabolic pathways for the different states. Positive rates indicate catabolic processes where ATP is produced, while negative rates indicate anabolic processes where ATP is consumed. Statistical significance is denoted as follows *, $P < 0.05$; **, $P < 0.01$; ***, $P < 0.001$; ****, $P < 0.0001$; ****, $P < 0.0001$.

**Supplementary Figure 3**

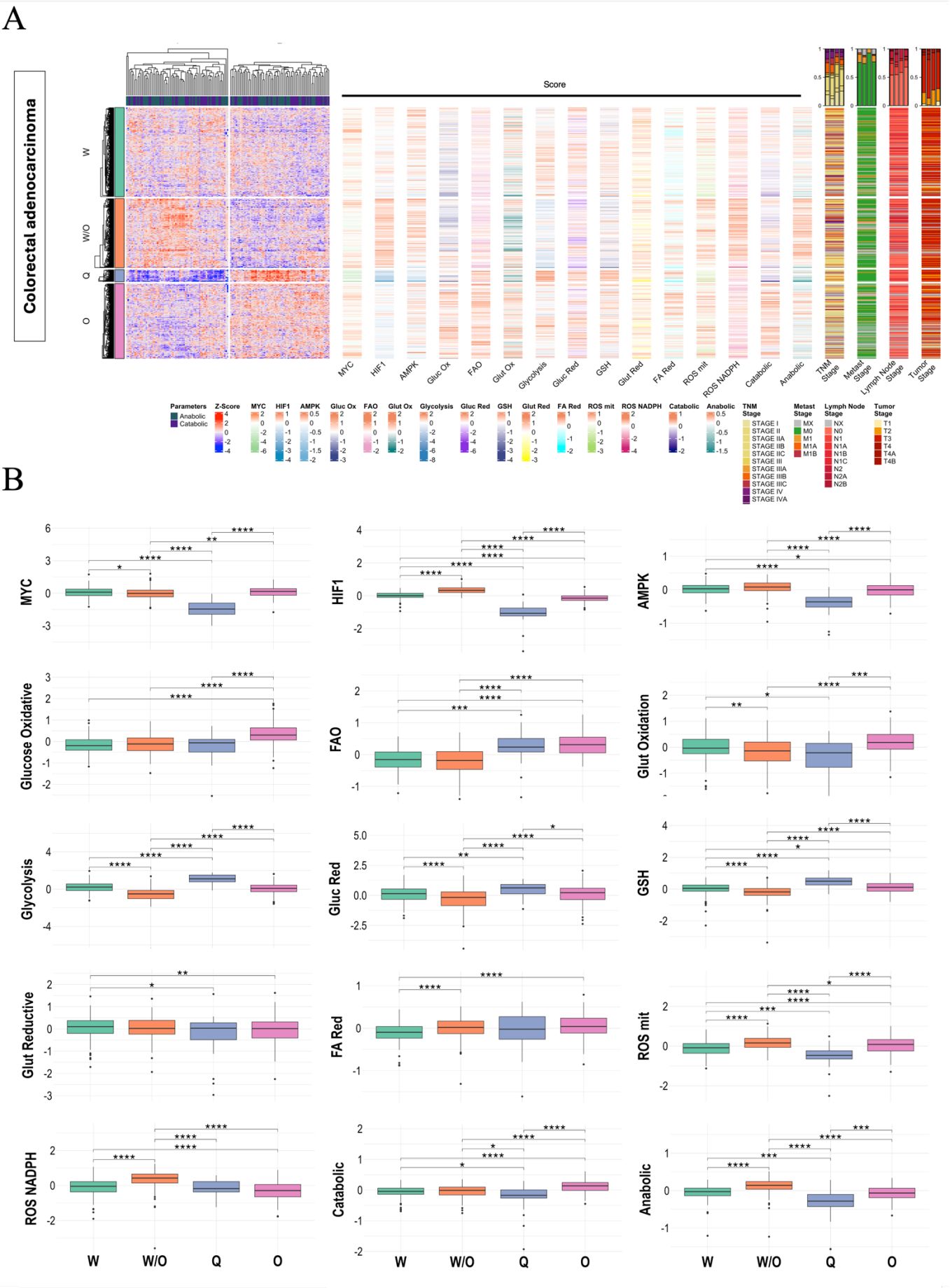

**Supplementary Figure 3. The association between gene activity and metabolic pathway activity for colorectal carcinoma**. **A.** Heatmap of RNA-seq data. Each row represents a patient sample, and each column represents the expression of selected genes, which are divided according to their metabolic or anabolic activities. Four distinct clusters can be identified in the heatmap. The adjacent one-column heatmaps represent the scores for Myc, HIF-1, AMPK, glycolysis, glucose oxidation, FAO, glutamine oxidation, glycolysis, glucose reduction, GSH, glutamine reduction, FA reduction, ROS mitochondrial, ROS NADPH, overall catabolic, and overall anabolic activities, respectively, we also included some of the phenotypic data of cancer: TNM stage, metastasis stage, lymph node stage, and tumor stage. **B.** Box plots summarizing and showing the differences in the scores according to each identified cluster. A t-test was used to test the significance of each pair of clusters. Significance levels are indicated as follows: *, $P < 0.05$; **, $P < 0.01$; ***, $P < 0.001$; ****, $P < 0.0001$.

**Supplementary Figure 4**

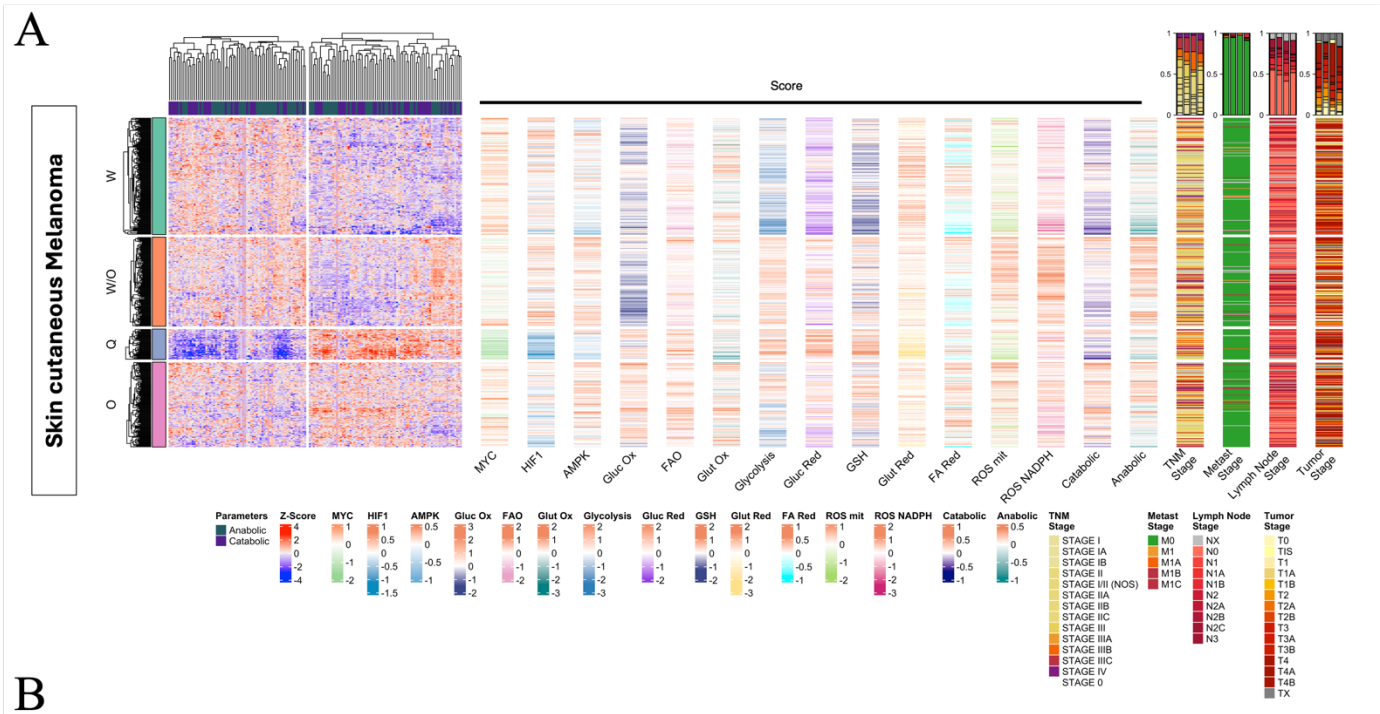


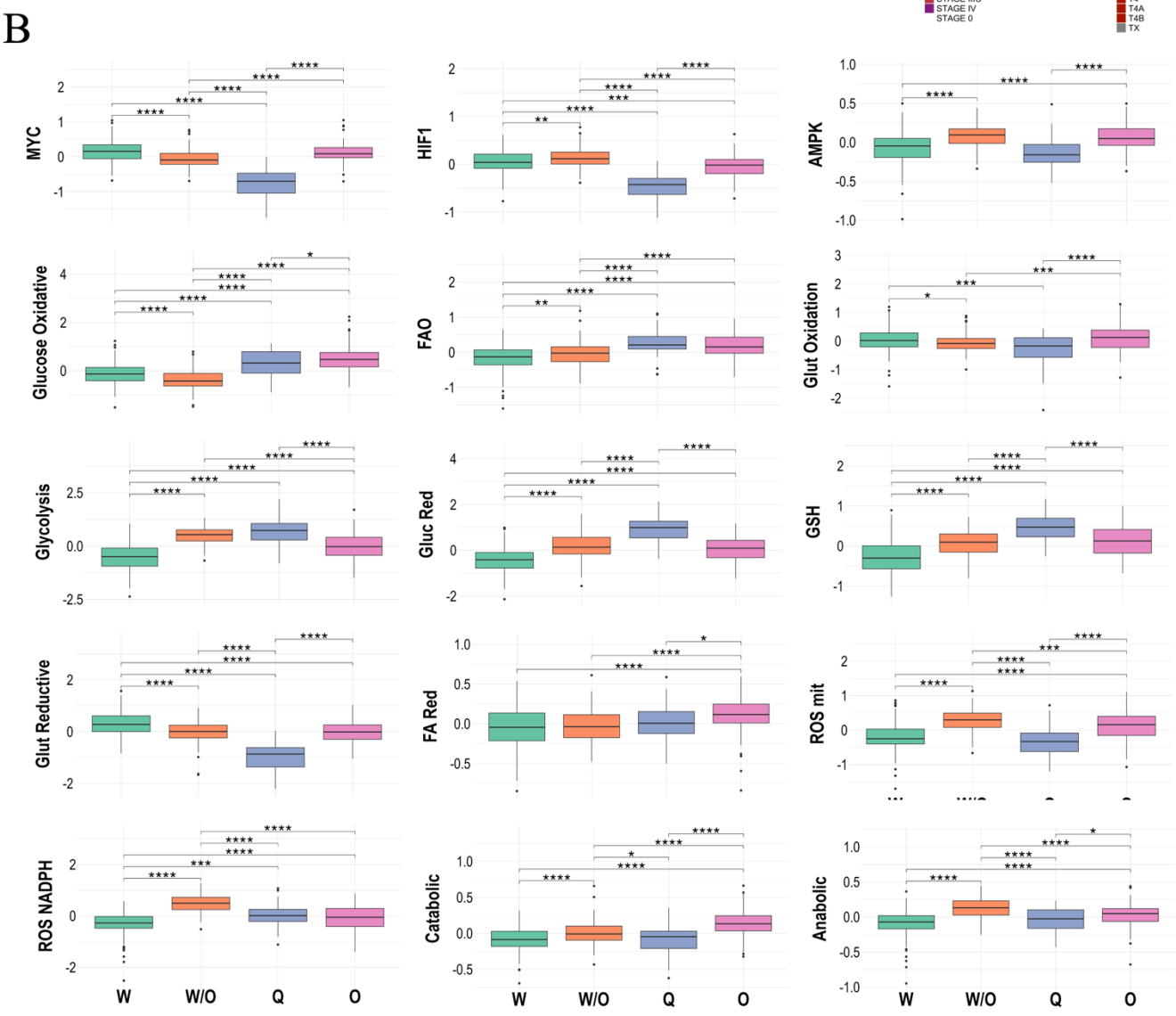

**Supplementary Figure 4. The association between gene activity and metabolic pathway activity for skin cutaneous melanoma**. **A.** Heatmap of RNA-seq data. Each row represents a patient sample, and each column represents the expression of selected genes, which are divided according to their metabolic or anabolic activities. Four distinct clusters can be identified in the heatmap. The adjacent one-column heatmaps represent the scores for Myc, HIF-1, AMPK, glycolysis, glucose oxidation, FAO, glutamine oxidation, glycolysis, glucose reduction, GSH, glutamine reduction, FA reduction, ROS mitochondrial, ROS NADPH, overall catabolic, and overall anabolic activities, respectively, we also included some of the phenotypic data of cancer: TNM stage, metastasis stage, lymph node stage, and tumor stage. **B.** Box plots summarizing and showing the differences in the scores according to each identified cluster. A t-test was used to test the significance of each pair of clusters. Significance levels are indicated as follows: *, $P < 0.05$; **, $P < 0.01$; ***, $P < 0.001$; ****, $P < 0.0001$.

**Supplementary Figure 5**

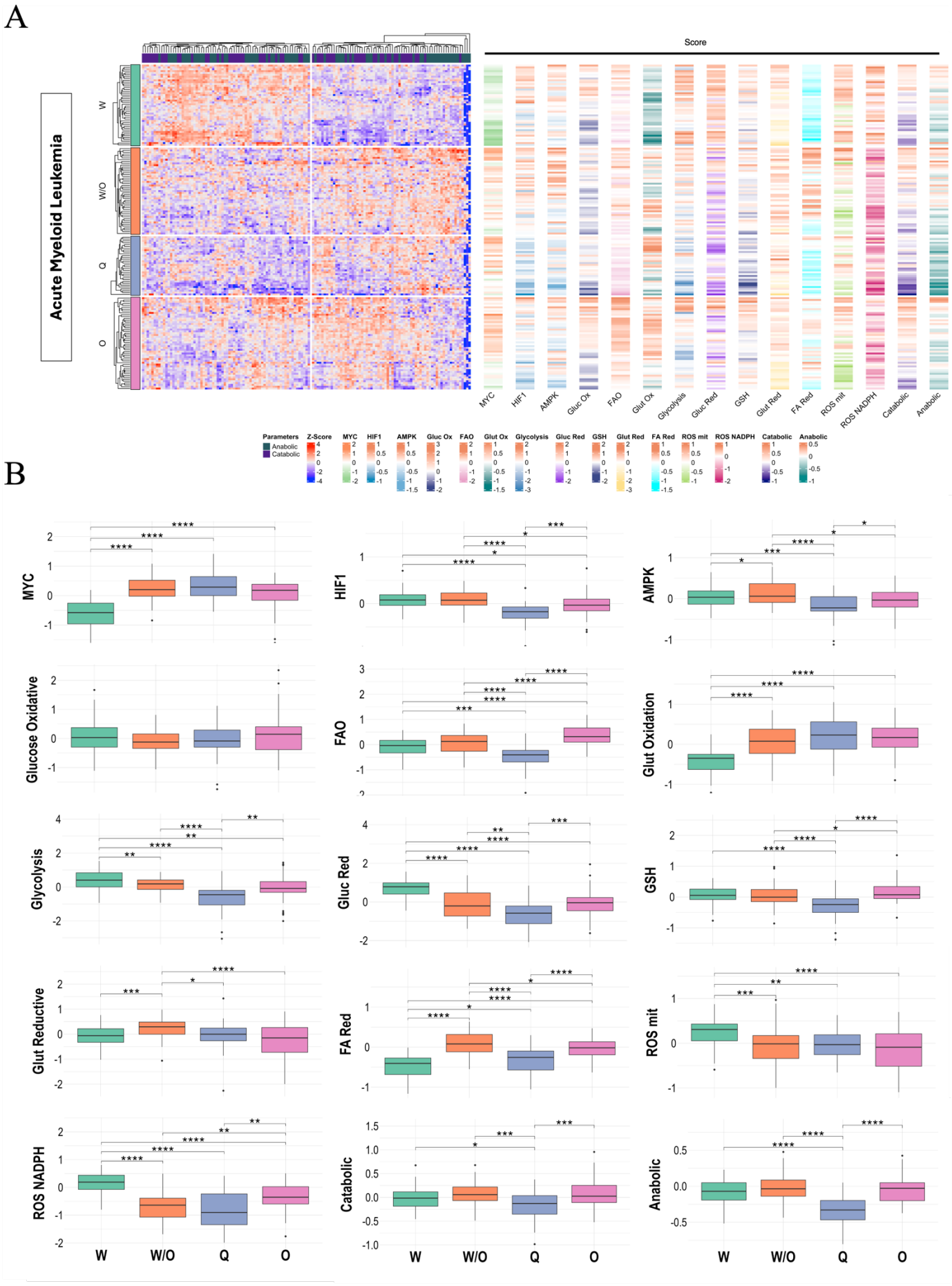

**Supplementary Figure 5. The association between gene activity and metabolic pathway activity for acute myeloid leukemia**. **A.** Heatmap of RNA-seq data. Each row represents a patient sample, and each column represents the expression of selected genes, which are divided according to their metabolic or anabolic activities. Four distinct clusters can be identified in the heatmap. The adjacent one-column heatmaps represent the scores for Myc, HIF-1, AMPK, glycolysis, glucose oxidation, FAO, glutamine oxidation, glycolysis, glucose reduction, GSH, glutamine reduction, FA reduction, ROS mitochondrial, ROS NADPH, overall catabolic, and overall anabolic activities, respectively, this data set did not include the phenotypic data analyzed for the rest of the cancers. **B.** Box plots summarizing and showing the differences in the scores according to each identified cluster. A t-test was used to test the significance of each pair of clusters. Significance levels are indicated as follows: *, $P < 0.05$; **, $P < 0.01$; ***, $P < 0.001$; ****, $P < 0.0001$.

78 **Supplementary Figure 6**

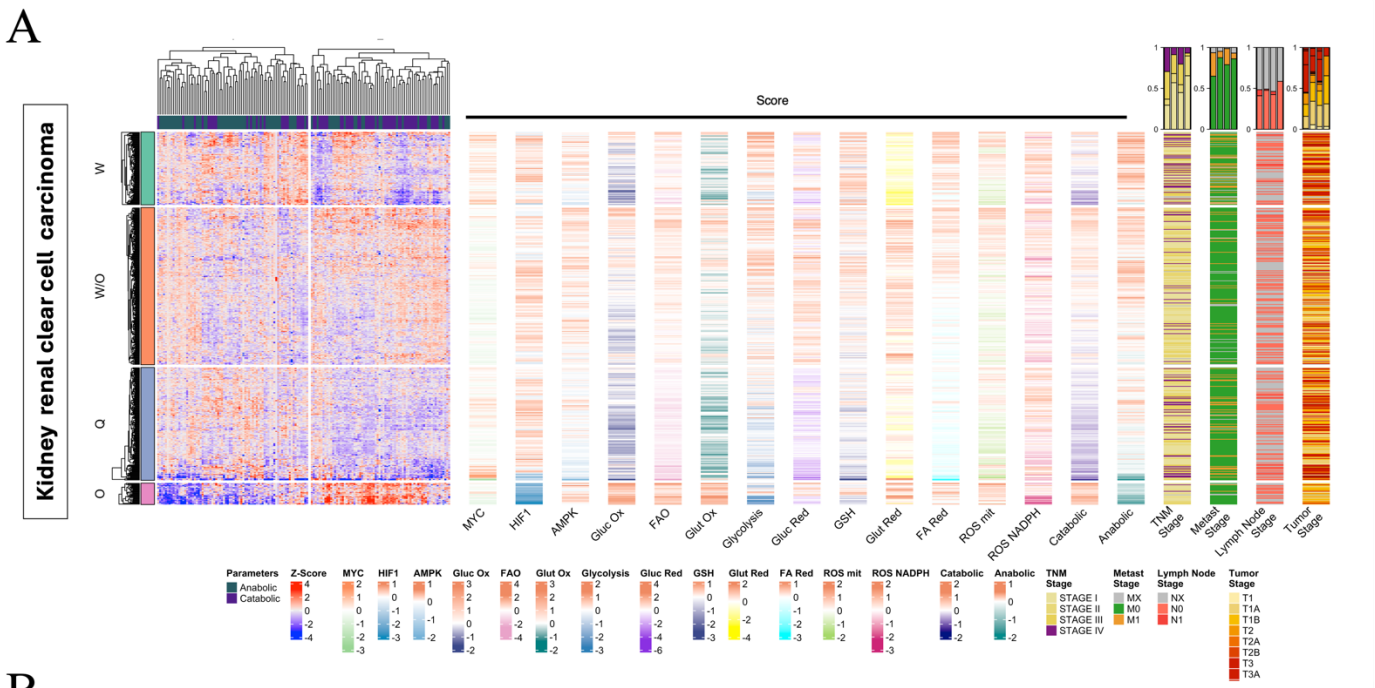


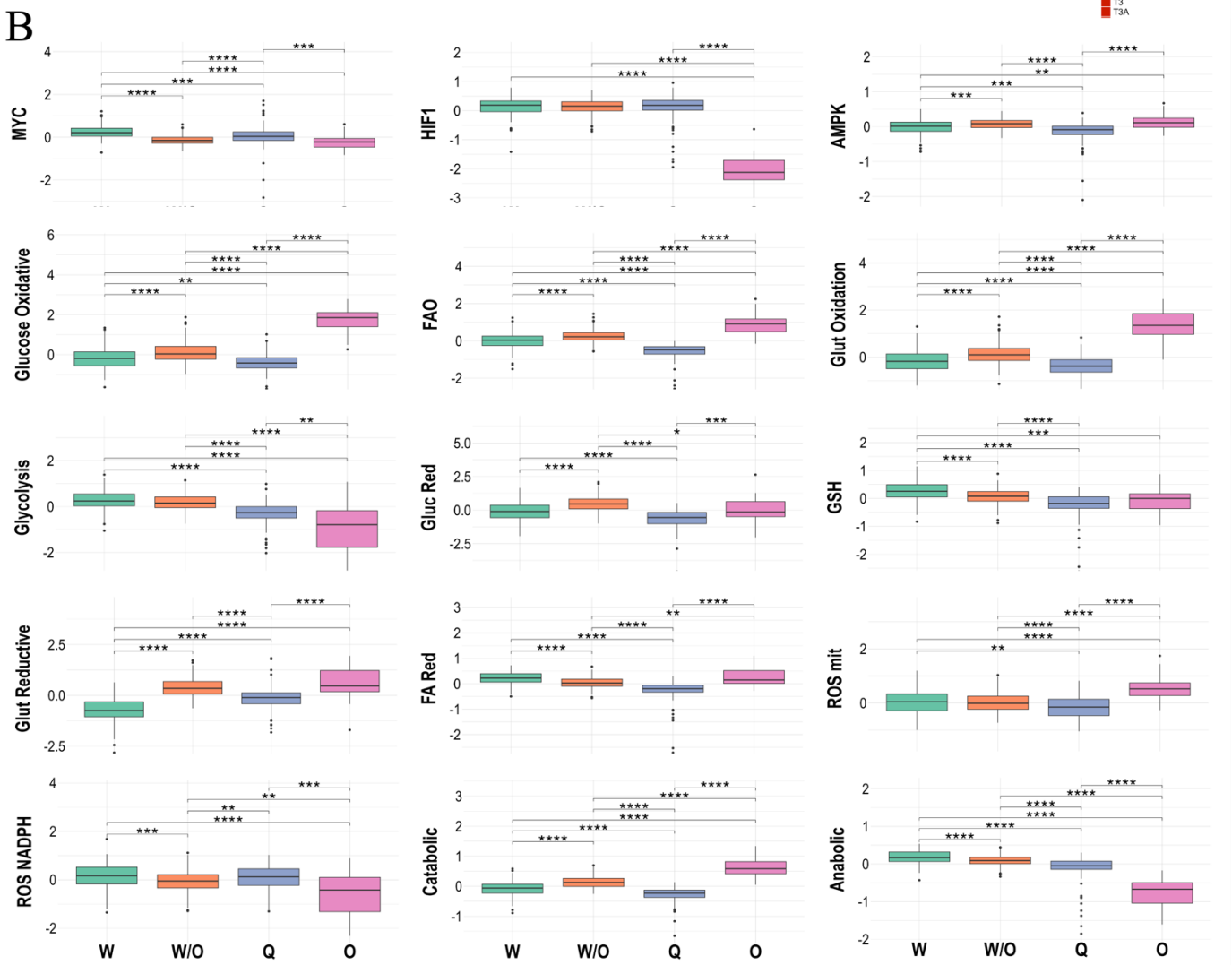


79

**Supplementary Figure 6. The association between gene activity and metabolic pathway activity for Kidney renal clear cell carcinoma**. **A.** Heatmap of RNA-seq data. Each row represents a patient sample, and each column represents the expression of selected genes, which are divided according to their metabolic or anabolic activities. Four distinct clusters can be identified in the heatmap. The adjacent one-column heatmaps represent the scores for Myc, HIF-1, AMPK, glycolysis, glucose oxidation, FAO, glutamine oxidation, glycolysis, glucose reduction, GSH, glutamine reduction, FA reduction, ROS mitochondrial, ROS NADPH, overall catabolic, and overall anabolic activities, respectively, we also included some of the phenotypic data of cancer: TNM stage, metastasis stage, lymph node stage, and tumor stage. **B.** Box plots summarizing and showing the differences in the scores according to each identified cluster. A t-test was used to test the significance of each pair of clusters. Significance levels are indicated as follows: *, $P < 0.05$; **, $P < 0.01$; ***, $P < 0.001$; ****, $P < 0.0001$.

**Supplementary Figure 7**

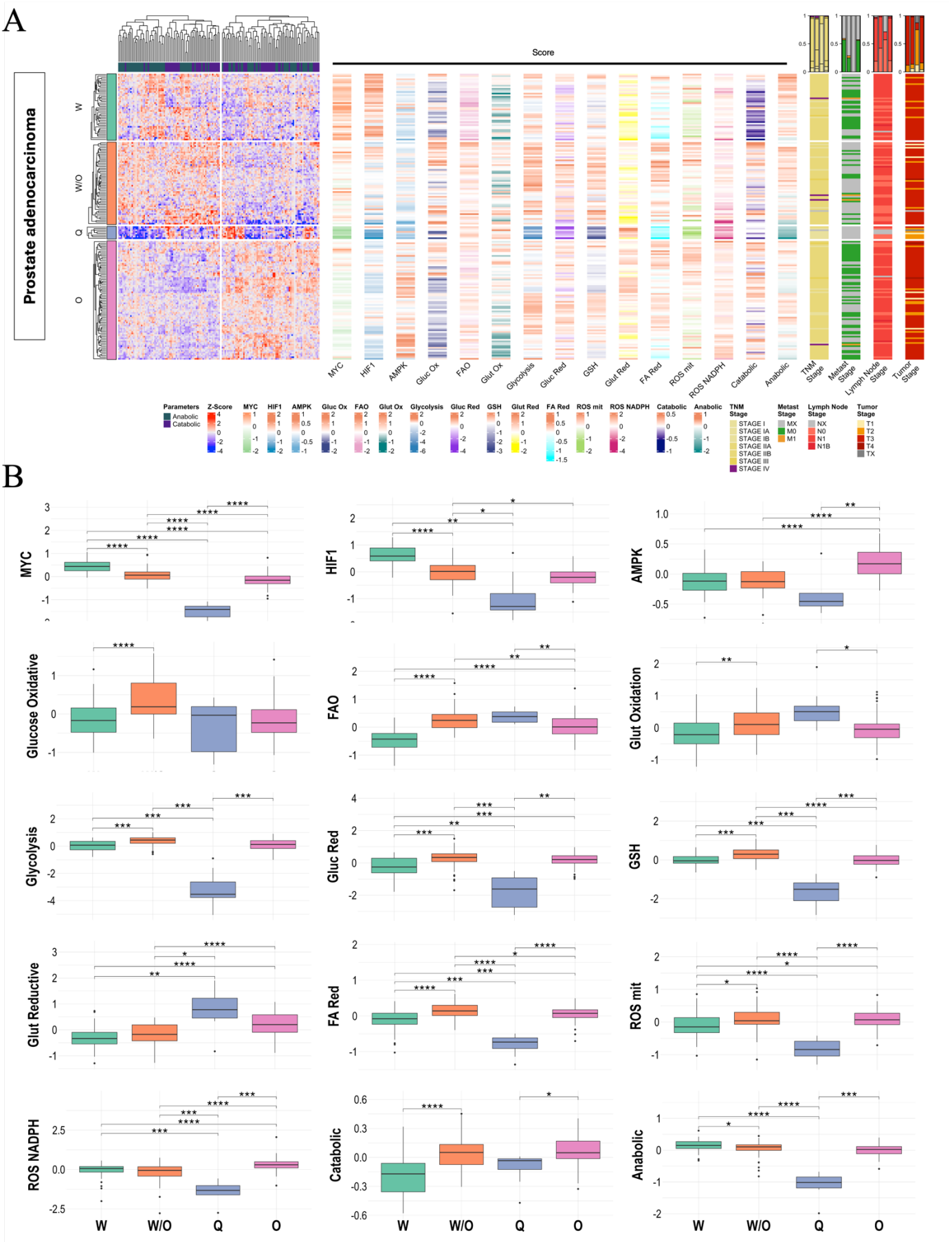

**Supplementary Figure 7. The association between gene activity and metabolic pathway activity for prostate adenocarcinoma**. **A.** Heatmap of RNA-seq data. Each row represents a patient sample, and each column represents the expression of selected genes, which are divided according to their metabolic or anabolic activities. Four distinct clusters can be identified in the heatmap. The adjacent one-column heatmaps represent the scores for Myc, HIF-1, AMPK, glycolysis, glucose oxidation, FAO, glutamine oxidation, glycolysis, glucose reduction, GSH, glutamine reduction, FA reduction, ROS mitochondrial, ROS NADPH, overall catabolic, and overall anabolic activities, respectively, we also included some of the phenotypic data of cancer: TNM stage, metastasis stage, lymph node stage, and tumor stage **B.** Box plots summarizing and showing the differences in the scores according to each identified cluster. A t-test was used to test the significance of each pair of clusters. Significance levels are indicated as follows: *, $P < 0.05$; **, $P < 0.01$; ***, $P < 0.001$; ****, $P < 0.0001$.

**Supplementary Figure 8**

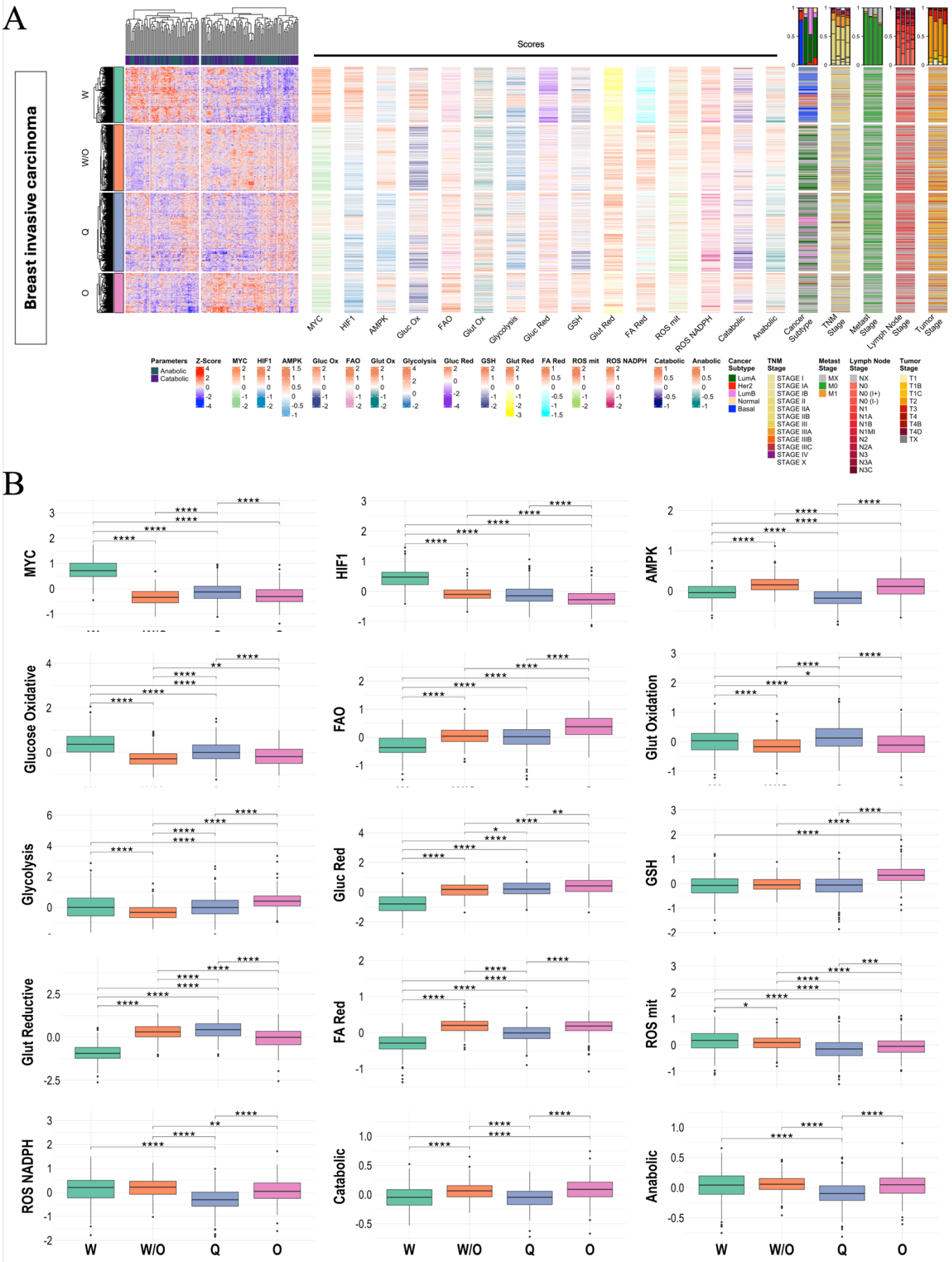

**Supplementary Fig 8: The association between gene activity and metabolic pathway activity for breast invasive carcinoma**. **A.** Heatmap of RNA-seq data. Each row represents a patient sample, and each column represents the expression of selected genes, which are divided according to their metabolic or anabolic activities. Four distinct clusters can be identified in the heatmap. The adjacent one-column heatmaps represent the scores for Myc, HIF-1, AMPK, glycolysis, glucose oxidation, FAO, glutamine oxidation, glycolysis, glucose reduction, GSH, glutamine reduction, FA reduction, ROS mitochondrial, ROS NADPH, overall catabolic, and overall anabolic activities, respectively, we also included some of the phenotypic data of cancer: cancer, subtype, TNM stage, metastasis stage, lymph node stage, and tumor stage **B.** Box plots summarizing and showing the differences in the scores according to each identified cluster. A t-test was used to test the significance of each pair of clusters. Significance levels are indicated as follows: *, $P < 0.05$; **, $P < 0.01$; ***, $P < 0.001$; ****, $P < 0.0001$.

**Supplementary Figure 9**

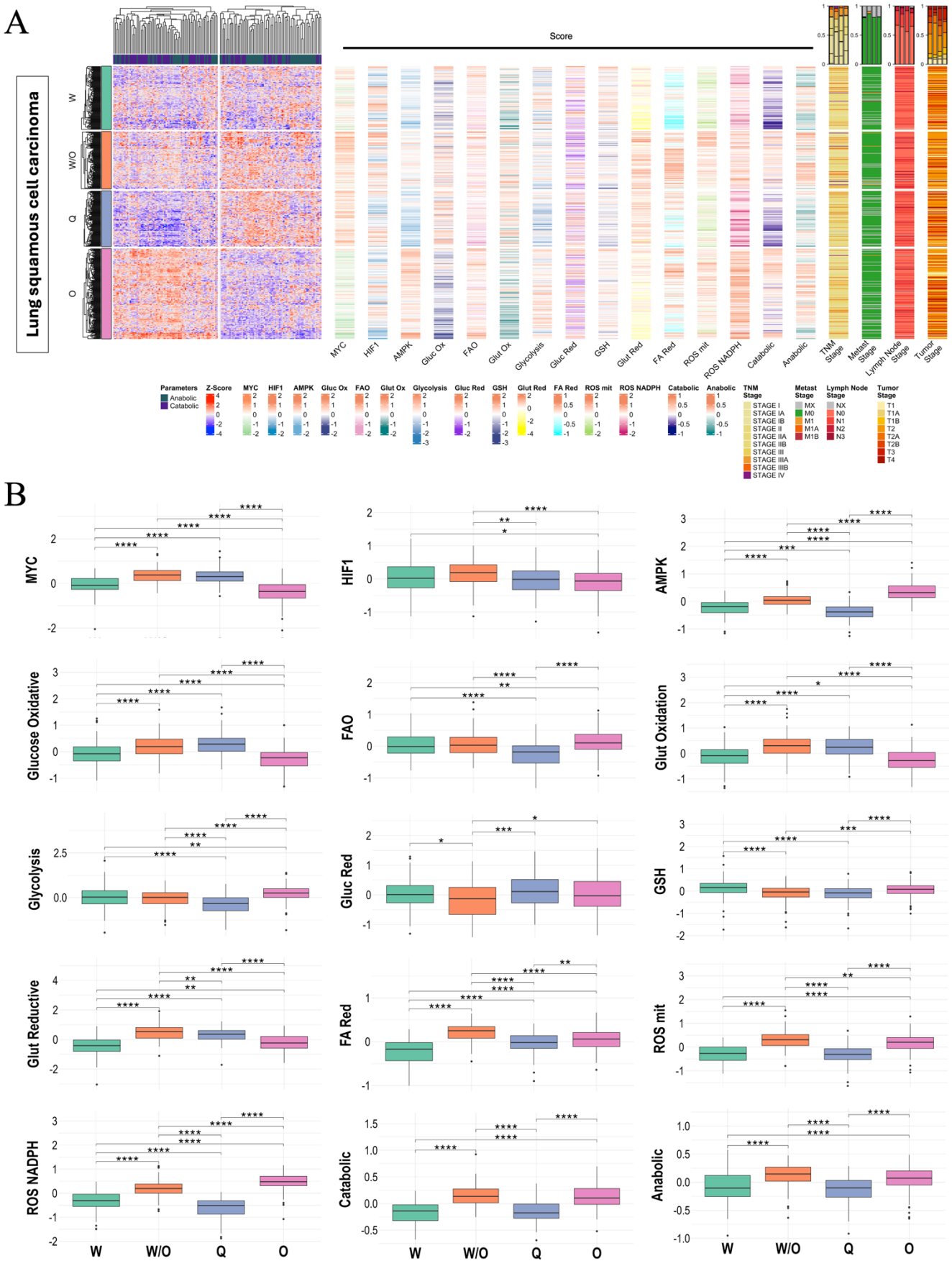

**Supplementary Figure 9. The association between gene activity and metabolic pathway activity for lung squamous cell carcinoma**. **A.** Heatmap of RNA-seq data. Each row represents a patient sample, and each column represents the expression of selected genes, which are divided according to their metabolic or anabolic activities. Four distinct clusters can be identified in the heatmap. The adjacent one-column heatmaps represent the scores for Myc, HIF-1, AMPK, glycolysis, glucose oxidation, FAO, glutamine oxidation, glycolysis, glucose reduction, GSH, glutamine reduction, FA reduction, ROS mitochondrial, ROS NADPH, overall catabolic, and overall anabolic activities, respectively, we also included some of the phenotypic data of cancer: TNM stage, metastasis stage, lymph node stage, and tumor stage. **B.** Box plots summarizing and showing the differences in the scores according to each identified cluster. A t-test was used to test the significance of each pair of clusters. Significance levels are indicated as follows: *, $P < 0.05$; **, $P < 0.01$; ***, $P < 0.001$; ****, $P < 0.0001$.

**Supplementary Figure 10**

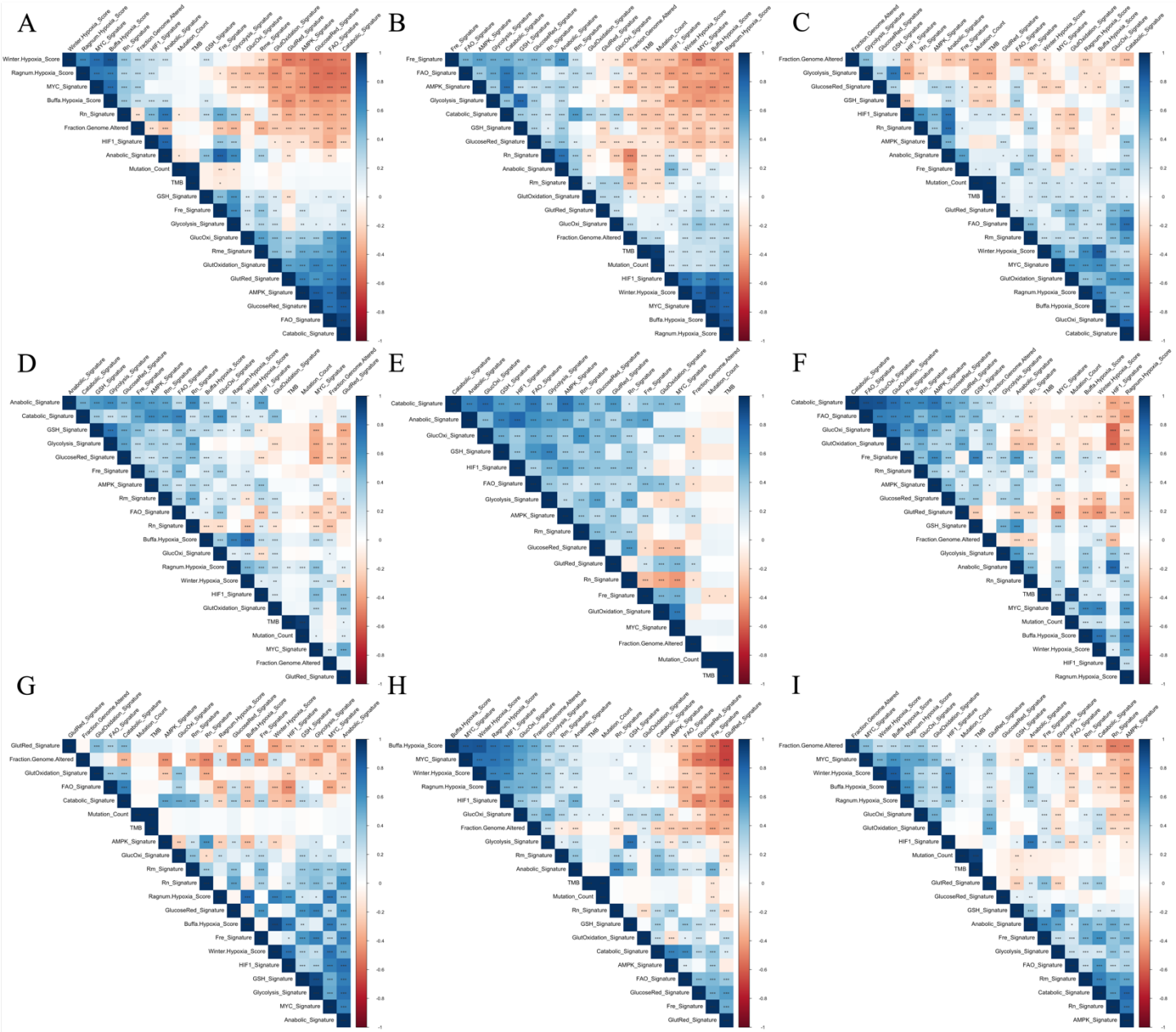


**Supplementary Figure 10. Correlograms of Metabolic Scores Across Various Cancer Types.** Correlograms between the metabolic scores for each cancer dataset were analyzed. The analysis includes the following cancer types: A. Hepatocellular carcinoma (LIHC), B. Lung adenocarcinoma (LUAD), C. Colorectal adenocarcinoma (COAD), D. Skin cutaneous melanoma (SKCM), E. Acute myeloid leukemia (LAML), F. Kidney renal clear cell carcinoma (KIRC), G. Prostate adenocarcinoma (PRAD), H. Breast invasive carcinoma (BRCA), and I. Lung squamous cell carcinoma (LUSC). The correlation matrix was computed, and the statistical significance of the correlations was assessed at a 95% confidence level. Significance levels are indicated as follows: *, $P < 0.05$; **, $P < 0.01$; ***, $P < 0.001$.

**Supplementary Figure 11**

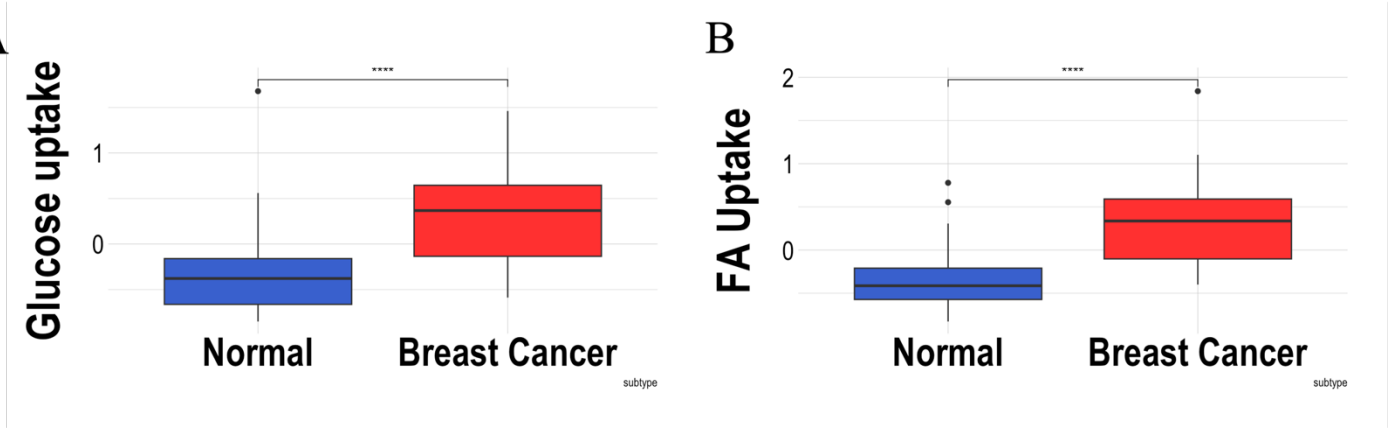


**Supplementary Figure 11:** Glucose uptake signature (A) and Fatty acid uptake score (B )were applied to a normal versus breast cancer dataset (1). T-test was used to test the significance *, $P < 0.05$; **, $P < 0.01$; ***, $P < 0.001$; ****, $P < 0.0001$. From the genes associated with both glucose and fatty acid (FA) uptake signatures, a differential gene expression analysis was performed as a first step to identify those specifically overexpressed in this specific cancer. The plots were generated using only the subset of genes that were overexpressed in cancer. While the original list included genes typically overexpressed in cancer, not all of them were applicable to this specific breast cancer dataset.

**Supplementary Figure 12**

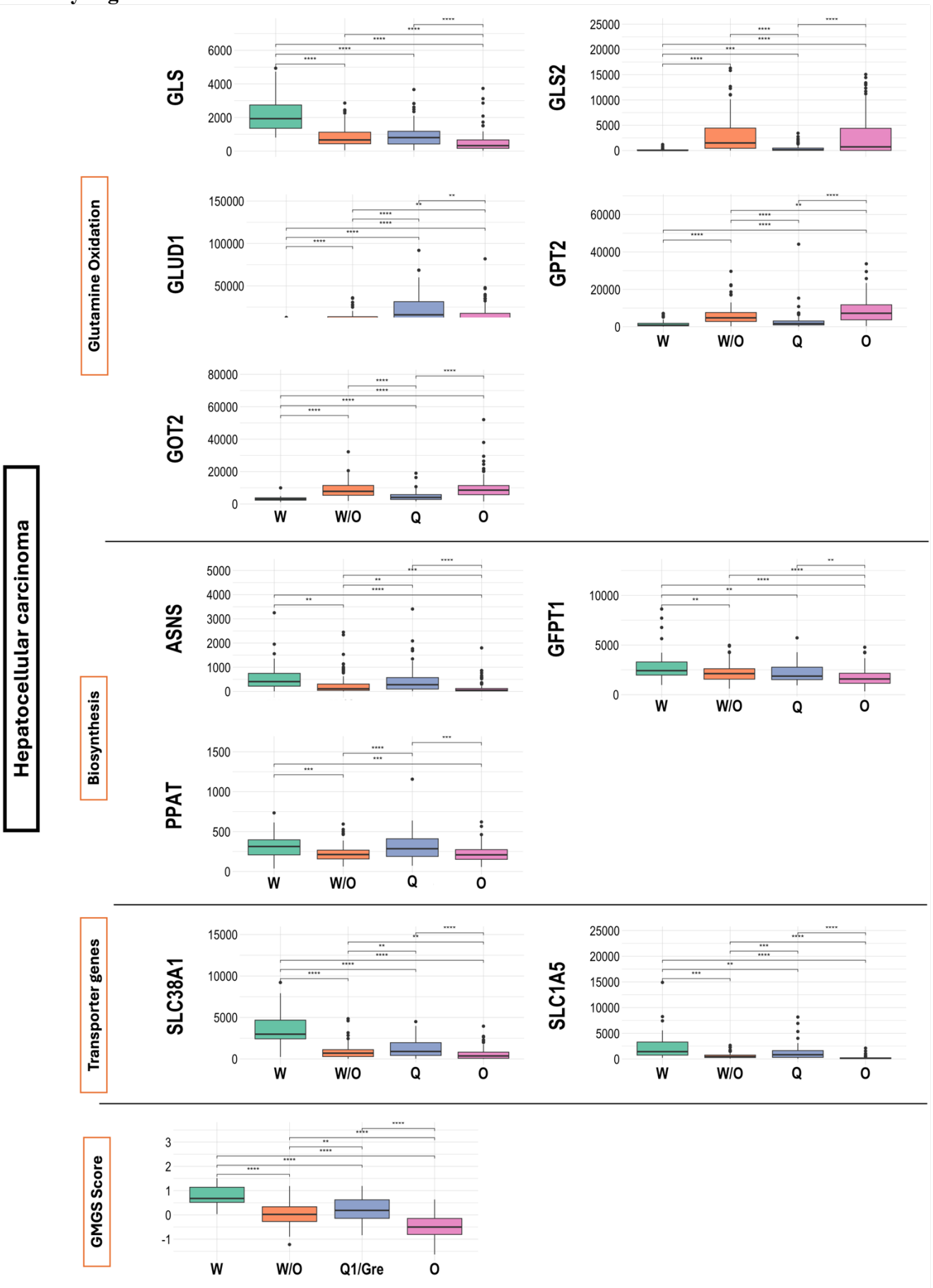

**Supplementary Figure 12. Comparison of glutamine metabolism relevant genes in the "O", "W", "W/O" and "Q" states in the hepatocellular carcinoma samples**. The glutamine metabolism relevant genes can be largely classified into three categories: oxidation genes (GLS, GLS2, GOT2, GLUD1 and GPT2), biosynthesis genes (ASNS, GFPT1, PPAT), and transporter genes (SLC38A1/2, SLC1A5), the gene signature (GMGS) is also included. T-test was used to test the significance *, $P < 0.05$; **, $P < 0.01$; ***, $P < 0.001$; ****, $P < 0.0001$.

**Supplementary Figure 13**

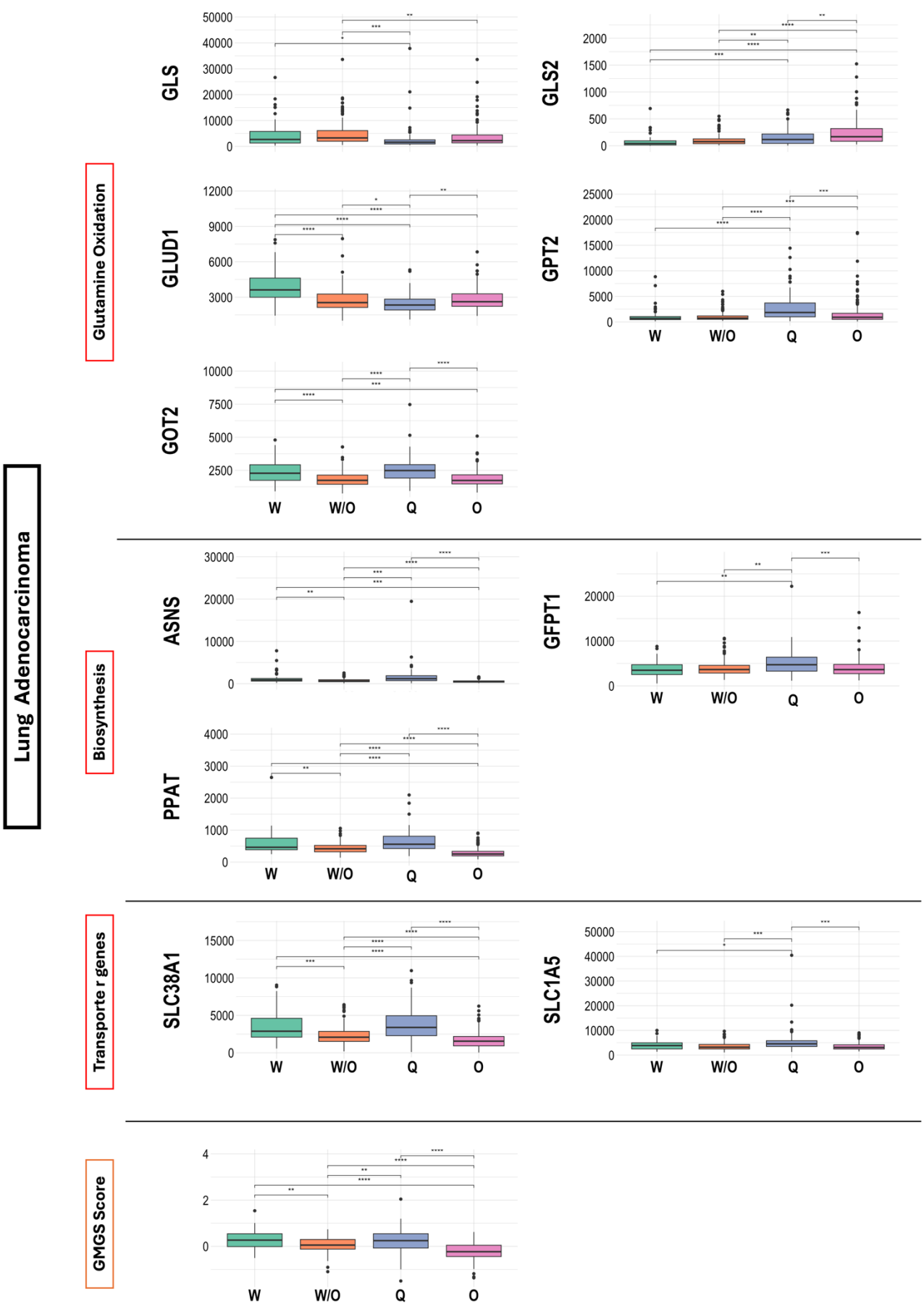

**Supplementary Figure 13. Comparison of glutamine metabolism relevant genes in the "O", "W", "W/O" and "Q" states in the Lung adenocarcinoma samples**. The glutamine metabolism relevant genes can be largely classified into three categories: oxidation genes (GLS, GLS2, GOT2, GLUD1 and GPT2), biosynthesis genes (ASNS, GFPT1, PPAT), and transporter genes (SLC38A1/2, SLC1A5), the gene signature (GMGS) is also included. T-test was used to test the significance *, $P < 0.05$; **, $P < 0.01$; ***, $P < 0.001$; ****, $P < 0.0001$.

**Supplementary Figure 14**

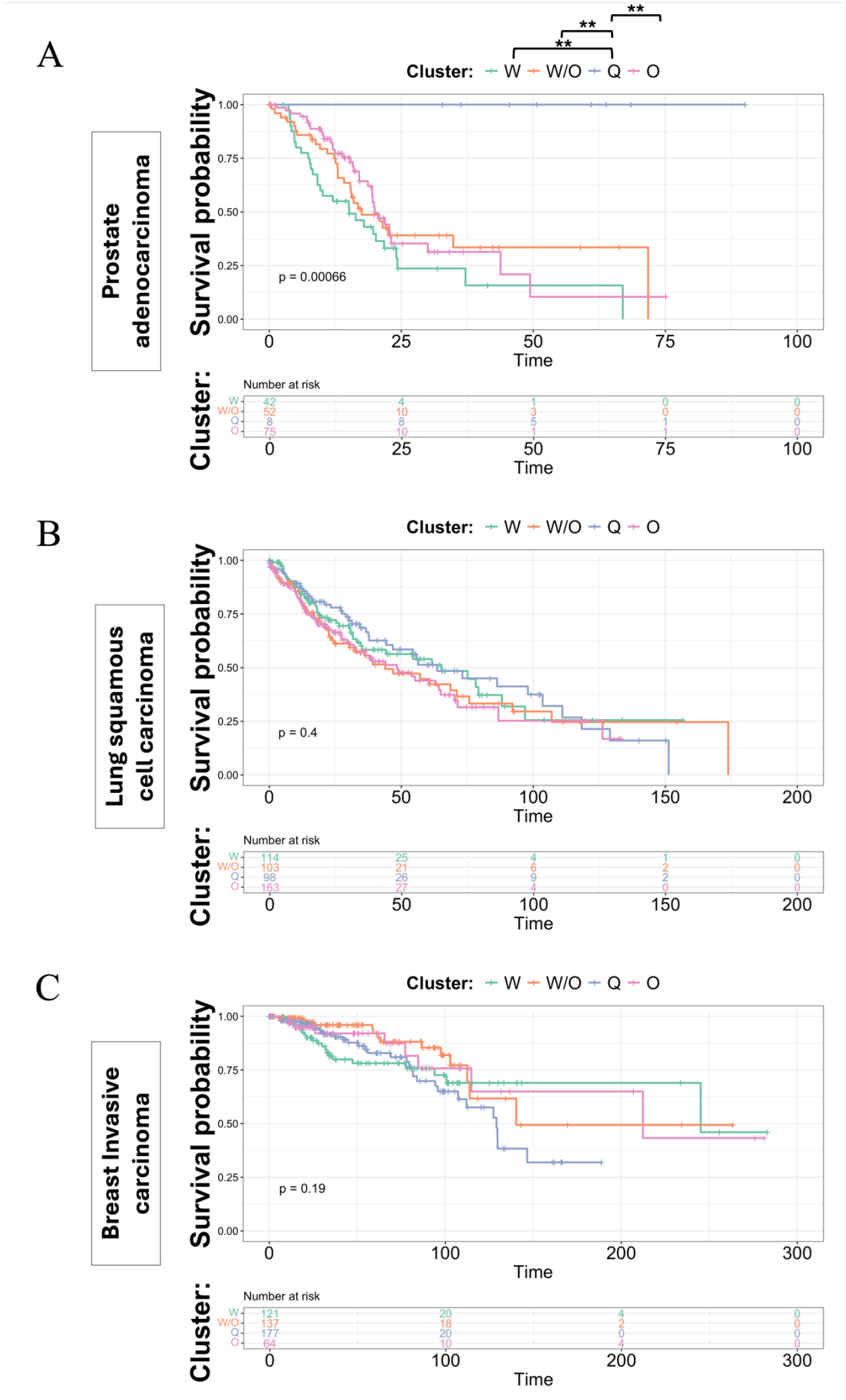

**Supplementary Figure 14 Survival curves stratified by cluster.** Survival curves for prostate adenocarcinoma (A), lung squamous cell carcinoma (B), and breast invasive carcinoma (C) datasets. Each dataset was separated in the four distinct phenotypes according to their metabolic or anabolic activities. The survival curves were estimated using the Kaplan-Meier method and compared using the log-rank test. Pairwise comparisons of survival distributions stratified by cluster are displayed above the survival curve for each pair of clusters. Significance levels are indicated as follows: *, $P < 0.05$; **, $P < 0.01$.

# Supplementary Figure 15

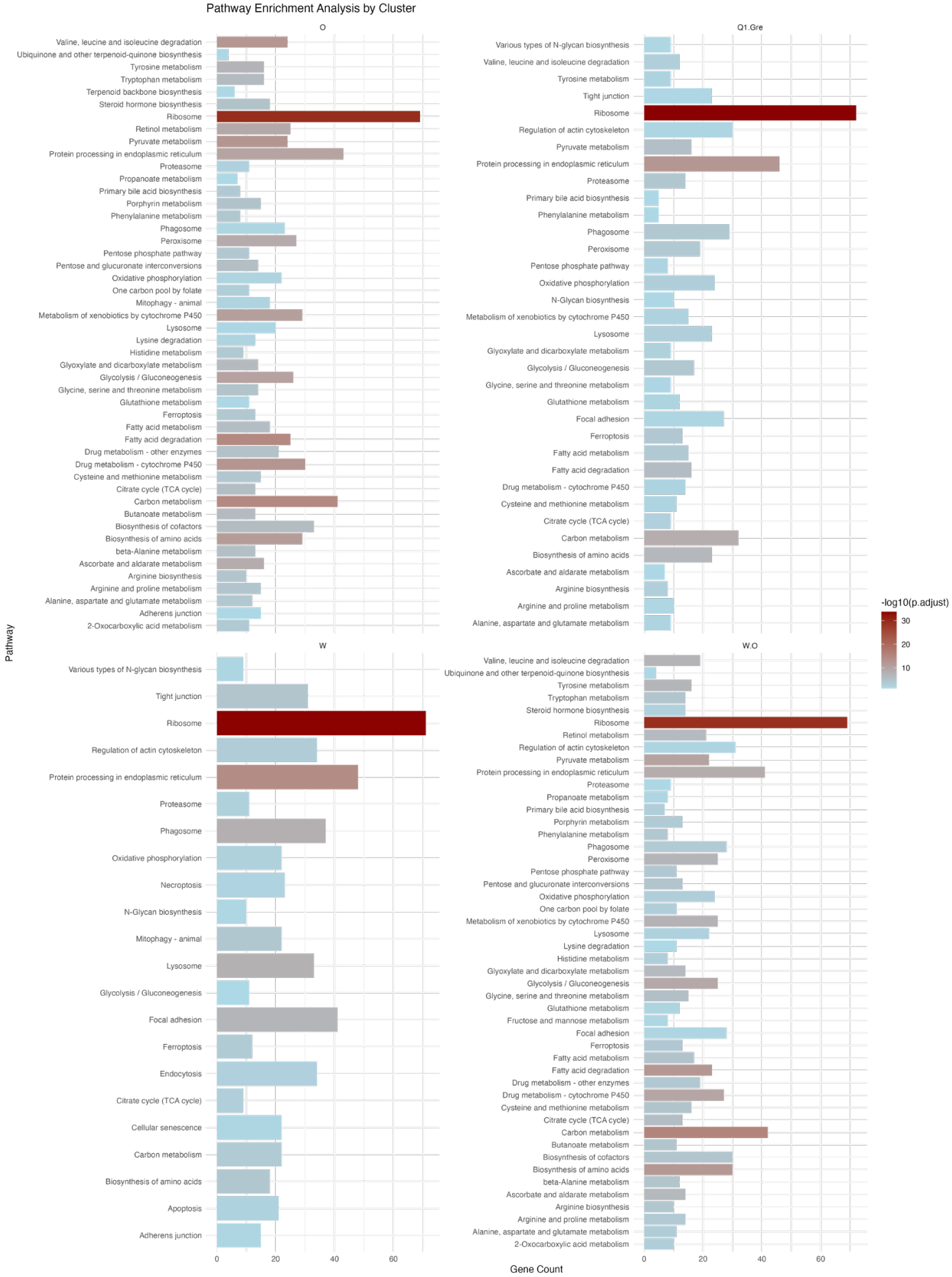

**Supplementary Figure 15 Pathway Enrichment Analysis by Cluster**. Bar plots show the results of KEGG pathway enrichment analysis for genes from different clusters (W, W/O, Q, O) from the LIHC data set. The x-axis represents the gene count in each enriched pathway, and the y-axis lists the pathways. The fill color of the bars corresponds to the significance of the enrichment, with darker red indicating stronger statistical significance (lower adjusted p-value). The values were obtained by first identifying the top 1000 most highly expressed genes from each cluster, followed by performing the KEGG enrichment analysis using the clusterProfiler package.

**Supplementary Figure 16**

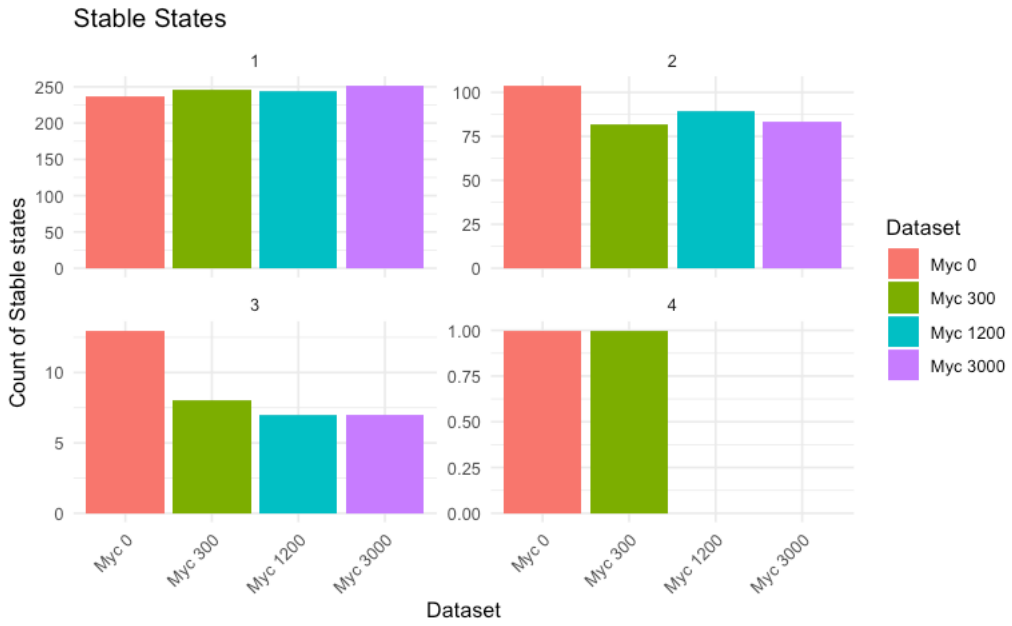


**Supplementary Figure 16 Count of the stable states obtained after the parameter randomization for each Myc level**. It highlights both monostable and multi-stable states. Although the occurrence of four stable states is less frequent, it remains a possibility within our model. The respective number of stable states per MYC level is as follows: 487 for MYC level 0, 438 for MYC level 300, 448 for MYC level 1200, and 439 for MYC level 3000

**Supplementary Table 1. The values of parameters**

| Parameters | Value | Unit | Description | Ref |
|---|---|---|---|---|
| $g_{R_{mt}}$ | 0.9 | $nmol \cdot L^{-1} \cdot h^{-1}$ | Production rate of mtROS | |
| $\gamma_{G_1}$ | 50 | - | mtROS production in glucose oxidation | |
| $\gamma_F$ | $\gamma_{G_1} * 9/2$ | - | mtROS production in fatty acid oxidation | |
| $\gamma_{Q_1}$ | 10 | - | mtROS production in glutamine oxidation | |
| $k_{R_{mt}}$ | 5 | $min^{-1}$ | Degradation rate of mtROS | (2,3) |
| $A^0_{R_{mt}}$ | 350 | $nmol \cdot L^{-1}$ | Threshold of mtROS inhibition by AMPK | (4) |
| $\lambda_{A,R_{mt}}$ | 2 | - | Fold change of mtROS inhibition by AMPK | |
| $n_{A,R_{mt}}$ | 2 | - | Hill coefficient | |
| $G^0_{GSH,R}$ | 10 | $\mu mol \cdot L^{-1} \cdot s^{-1}$ | Threshold of mtROS clearance by AMPK | |
| $\lambda_{GSH,R}$ | 1.2 | - | Fold change of mtROS clearance by AMPK | |
| $n_{GSH,R}$ | 2 | - | Hill coefficient | |
| $g_{R_{nox}}$ | 40 | $\mu mol \cdot L^{-1} \cdot min^{-1}$ | Production rate of noxROS | (2,3) |
| $g_0$ | 1 | - | Basal noxROS | |
| $g_{H,R_{nox}}$ | 5 | - | Fold-change of noxROS activation by HIF-1 | (5) |
| $H^0_{R_{nox}}$ | 250 | $nmol \cdot L^{-1}$ | Threshold of noxROS activation by HIF-1 | |
| $n_{H,R_{nox}}$ | 2 | - | Hill coefficient | (5) |

| | | | | |
|---|---|---|---|---|
| $g_{A,R_{nox}}$ | 0.2 | - | Fold change of noxROS inhibition by AMPK | (5) |
| $A^0_{R_{nox}}$ | 150 | $nmol \cdot L^{-1}$ | Threshold of noxROS inhibition by AMPK | (4) |
| $n_{A,R_{nox}}$ | 2 | - | Hill coefficient | (5) |
| $k_{R_{nox}}$ | 5 | $min^{-1}$ | Degradation rate of noxROS | (2,3) |
| $g_A$ | 40 | $nmol \cdot L^{-1} \cdot h^{-1}$ | Production rate of AMPK | |
| $R^0_{T,A}$ | 250 | $\mu mol \cdot L^{-1}$ | Threshold of AMPK activation by ROS | |
| $\lambda_{R_T,A}$ | 8 | - | Fold change of AMPK activation by ROS | (6) |
| $n_{R_T,A}$ | 4 | - | Hill coefficient | (5) |
| $H^0_A$ | 150 | $nmol \cdot L^{-1}$ | Threshold of AMPK inhibition by HIF-1 | |
| $\lambda_{H,A}$ | 0.1 | - | Fold-change of AMPK inhibition by HIF-1 | (5) |
| $n_{H,A}$ | 1 | - | Hill coefficient | (5) |
| $\lambda_{X_{ATP},A}$ | 0.25 | - | Fold-change of AMPK inhibition by ATP | |
| $X^0_{ATP,A}$ | 2000 | $\mu mol \cdot L^{-1} \cdot s^{-1}$ | Threshold of AMPK inhibition by ATP | |
| $n_{X_{ATP},A}$ | 2 | - | Hill coefficient | (5) |
| $k_A$ | 0.2 | $h^{-1}$ | Degradation rate of AMPK | (5) |
| $g_H$ | 15 | $nmol \cdot L^{-1} \cdot h^{-1}$ | Production rate of HIF-1 | (7) |
| $A^0_H$ | 150 | $nmol \cdot L^{-1}$ | Threshold of HIF-1 inhibition by AMPK | |
| $\lambda_{A,H}$ | 0.1 | - | Fold-change of HIF-1 inhibition by AMPK | (5) |

| | | | | |
|---|---|---|---|---|
| $n_{A,H}$ | 1 | - | Hill coefficient | |
| $k_H$ | 0.25 | $h^{-1}$ | Degradation rate of HIF-1 | (7) |
| $G^0_{2,H}$ | 250 | $\mu mol \cdot L^{-1} \cdot s^{-1}$ | Threshold of HIF-1 activation by glycolysis | |
| $\lambda_{G_2,H}$ | 0.1 | - | Fold-change of HIF-1 activation by glycolysis | |
| $n_{G_2,H}$ | 4 | - | Hill coefficient | |
| $M$ | 0-3000 | $\mu mol \cdot L^{-1}$ | Myc Level | |
| $M^0_{M,H}$ | 150 | $\mu mol \cdot L^{-1} \cdot s^{-1}$ | Threshold of MYC inhibiting HIF-1 degradation | |
| $\lambda_{M,H}$ | 0.8 | - | Fold change of MYC inhibiting HIF-1 degradation | |
| $n_{M,H}$ | 2 | - | Hill coefficient | |
| $\lambda_{R_T,H}$ | 0.2 | - | Fold-change of HIF-1 stabilization by ROS | (5) |
| $R^0_{T,H}$ | 40 | $\mu mol \cdot L^{-1}$ | Threshold of HIF-1 stabilization by ROS | |
| $n_{R_T,H}$ | 4 | - | Hill coefficient | (5) |
| $g_{H,G_0}$ | 20 | $\mu mol \cdot L^{-1} \cdot s^{-1}$ | Basal glucose uptake rate | |
| $H^0_{G_0}$ | 150 | $nmol \cdot L^{-1}$ | Threshold of glucose uptake regulated by HIF-1 | |
| $\lambda_{H,G_0}$ | 6 | - | Fold-change of glucose uptake regulated by HIF-1 | |
| $n_{H,G_0}$ | 4 | - | Hill coefficient | |
| $g_{A,G_0}$ | 20 | $\mu mol \cdot L^{-1} \cdot s^{-1}$ | Basal glucose uptake rate | |
| $A^0_{G_0}$ | 200 | $nmol \cdot L^{-1}$ | Threshold of glucose uptake regulated by AMPK | |

| | | | | |
|---|---|---|---|---|
| $\lambda_{A,G_0}$ | 4 | - | Fold-change of glucose uptake regulated by AMPK | |
| $n_{A,G_0}$ | 2 | - | Hill coefficient | |
| $M_{G_0}^0$ | 150 | $\mu mol \cdot L^{-1} \cdot s^{-1}$ | Threshold of glucose uptake regulated by MYC | |
| $\lambda_{M,G_0}$ | 2 | - | Fold change of glucose uptake regulated by MYC | |
| $n_{M,G_0}$ | 2 | - | Hill coefficient | |
| $M_{Q_0}^0$ | 150 | $\mu mol \cdot L^{-1} \cdot s^{-1}$ | Threshold of glutamine uptake regulated by MYC | |
| $\lambda_{M,Q_0}$ | 2 | - | Fold-change of glutamine uptake regulated by MYC | |
| $n_{M,Q_0}$ | 2 | - | Fold-change of glucose uptake regulated by MYC | |
| $g_{A,C_0}$ | 15 | $\mu mol \cdot L^{-1} \cdot s^{-1}$ | Basal utilization rate of acetyl-CoA for OXPHOS | |
| $A_{C_0}^0$ | 250 | $nmol \cdot L^{-1}$ | Threshold of acetyl-CoA utilization regulated by AMPK | |
| $\lambda_{A,C_0}$ | 8 | - | Fold-change of acetyl-CoA utilization regulated by AMPK | |
| $n_{A,C_0}$ | 4 | - | Hill coefficient | |
| $g_{G_1}$ | 100 | $\mu mol \cdot L^{-1} \cdot s^{-1}$ | Basal glucose oxidation rate | |
| $\lambda_{G,G_1}$ | 0.1 | - | Restriction of glucose oxidation rate by glucose uptake rate | |
| $n_{G,G_1}$ | 2 | - | Hill coefficient | |
| $\lambda_{C,G_1}$ | 0.1 | - | Restriction of glucose oxidation by acetyl-CoA utilization rate | |
| $n_{C,G_1}$ | 4 | - | Hill coefficient | |
| $g_{G_2}$ | 150 | $\mu mol \cdot L^{-1} \cdot s^{-1}$ | Basal glycolysis rate | |

| | | | | |
|---|---|---|---|---|
| $\lambda_{G,G_2}$ | 0.1 | - | Restriction of glycolysis rate by glucose uptake rate | |
| $n_{G,G_2}$ | 2 | - | Hill coefficient | |
| $H^0_{G_2}$ | 200 | $nmol \cdot L^{-1}$ | Threshold of glycolysis upregulation by HIF-1 | |
| $\lambda_{H,G_2}$ | 8 | - | Fold-change of glycolysis upregulation by HIF-1 | |
| $n_{H,G_2}$ | 4 | - | Hill coefficient | |
| $g_{G_r}$ | 60 | $nmol \cdot L^{-1} \cdot h^{-1}$ | Basal reductive glucose metabolic rate | |
| $\lambda_{G,G_{re}}$ | 0.1 | - | Restriction of reductive glucose metabolic rate by glucose uptake rate | |
| $n_{G,G_{re}}$ | 2 | - | Hill coefficient | |
| $A^0_{G_{re}}$ | 200 | $\mu mol \cdot L^{-1} \cdot s^{-1}$ | Threshold of reductive glucose metabolism regulation by AMPK | |
| $\lambda_{A,G_{re}}$ | 0.25 | - | Fold-change of reductive glucose metabolism regulation by AMPK | |
| $n_{A,G_{re}}$ | 2 | - | Hill coefficient | |
| $M^0_{G_{re}}$ | 150 | $\mu mol \cdot L^{-1} \cdot s^{-1}$ | Threshold of reductive glucose metabolism regulation by MYC | |
| $\lambda_{M,G_{re}}$, | 2 | - | Fold-change of reductive glucose metabolism regulation by MYC | |
| $n_{M,G_{re}}$ | 2 | - | Hill coefficient | |
| $g_f$ | 3 | $\mu mol \cdot L^{-1} \cdot s^{-1}$ | Basal FAO rate | |
| $\lambda_{C,F}$ | 0.1 | - | Restriction of FAO rate by acetyl-CoA utilization rate | |
| $n_{C,F}$ | 2 | - | Hill coefficient | |
| $A^0_{F_1}$ | 200 | $nmol \cdot L^{-1}$ | Threshold of FAO upregulation by AMPK | |

| | | | | |
|---|---|---|---|---|
| $\lambda_{A,F_1}$ | 6 | - | Fold-change of FAO upregulation by AMPK | |
| $n_{A,F_1}$ | 4 | - | Hill coefficient | |
| $g_{F0}$ | 5 | $mol \cdot L^{-1} \cdot s^{-1}$ | Basic fatty acid update rate | |
| $A^0_{F_0}$ | 200 | $\mu mol \cdot L^{-1} \cdot s^{-1}$ | Threshold of fatty acid uptake regulation by AMPK | |
| $n_{A,F_0}$ | 2 | - | Hill coefficient | |
| $\lambda_{A,F_0}$ | 4 | - | Fold-change of fatty acid uptake regulation by AMPK | |
| $\lambda_{F,F_1}$ | 0.8 | - | Restriction of FAO rate by fatty acid uptake rate | |
| $n_{F,F_1}$ | 2 | - | Hill coefficient | |
| $H^0_F$ | 200 | $\mu mol \cdot L^{-1} \cdot s^{-1}$ | Threshold of FAO regulation by HIF-1 | |
| $\lambda_{H,F}$, | 0.8 | - | Fold-change of FAO regulation by HIF-1 | |
| $n_{H,F}$ | 4 | - | Hill coefficient | |
| $\gamma_{G,F}$ | 0.1 | - | Lipogenesis rate of glucose | |
| $\gamma_{G,Q}$ | 0.1 | - | Lipogenesis rate of glutamine | |
| $g_{F_r}$ | 75 | $nmol \cdot L^{-1} \cdot h^{-1}$ | Basal reductive fatty acid metabolic rate | |
| $\lambda_{F,F_r}$ | 0.1 | - | Restriction of FAO rate by fatty acid uptake rate | |
| $n_{F,F_r}$ | 2 | - | Hill coefficient | |
| $g_{Q_1}$ | 30 | $nmol \cdot L^{-1} \cdot h^{-1}$ | Basal glutamine oxidation rate | |
| $\gamma_{GSH}$ | 0.1 | - | Effect of glutathione (GSH) on ROS. | |

| | | | | |
|---|---|---|---|---|
| $H_{Q_1}^0$ | 350 | $\mu mol \cdot L^{-1} \cdot s^{-1}$ | Threshold of glutamine oxidation regulation by HIF-1 | |
| $\lambda_{H,Q_1}$ | 0.2 | - | Fold change of glutamine oxidation regulation by HIF-1 | |
| $n_{H,Q_1}$ | 4 | - | Hill coefficient | |
| $\lambda_{Q,Q_1}$ | 0.5 | - | Restriction of glutamine oxidation rate by glutamine uptake rate | |
| $n_{Q,Q_1}$ | 2 | - | Hill coefficient | |
| $g_{Q_0}$ | 10 | $nmol \cdot L^{-1} \cdot h^{-1}$ | Basal glutamine update rate | |
| $M_{Q_0}^0$ | 150 | $nmol \cdot L^{-1}$ | Threshold of glutamine uptake regulation by MYC | |
| $\lambda_{M,Q_0}$ | 2 | - | Fold change of glutamine uptake regulation by MYC | |
| $n_{M,Q_0}$ | 2 | - | Hill coefficient | |
| $M_{Q_1}^0$ | 150 | $\mu mol \cdot L^{-1} \cdot s^{-1}$ | Threshold of glutamine oxidation regulation by MYC | |
| $\lambda_{M,Q_1}$ | 2 | - | Fold change of glutamine oxidation regulation by MYC | |
| $n_{M,Q_1}$ | 2 | - | Hill coefficient | |
| $g_{Q_{GSH}}$ | 30 | $nmol \cdot L^{-1} \cdot h^{-1}$ | Basal glutathione synthesis rate | |
| $\lambda_{Q,Q_{GSH}}$ | 0.5 | - | Restriction of glutathione synthesis rate by glutamine uptake rate | |
| $n_{Q,Q_{GSH}}$ | 2 | - | Hill coefficient | |
| $M_{Q_{GSH}}^0$ | 150 | $\mu mol \cdot L^{-1} \cdot s^{-1}$ | Threshold of glutathione synthesis regulation by MYC | |
| $\lambda_{M,Q_{GSH}}$ | 0.9 | - | Fold change of glutathione synthesis regulation by MYC | |
| $n_{M,Q_{GSH}}$ | 2 | - | Hill coefficient | |

| | | | | |
|---|---|---|---|---|
| $k_{GSH}$ | 1 | $h^{-1}$ | The decay rate of glutathione | |
| $g_{Q_r}$ | 20 | $nmol \cdot L^{-1} \cdot h^{-1}$ | Basal reductive glutamine metabolic rate | |
| $\lambda_{Q,Q_r}$ | 0.5 | - | Restriction of reductive glutamine metabolic rate by glutamine uptake rate | |
| $n_{Q,Q_r}$ | 2 | - | Hill coefficient | |
| $M_{Q_r}^0$ | 150 | $\mu mol \cdot L^{-1} \cdot s^{-1}$ | Threshold of reductive glutamine metabolism regulation by MYC | |
| $\lambda_{M,Q_r}$ | 2 | - | Fold change of reductive glutamine metabolism regulation by MYC | |
| $n_{M,Q_r}$ | 2 | - | Hill coefficient | |
| $H_{Q_r}^0$ | 200 | $\mu mol \cdot L^{-1} \cdot s^{-1}$ | Threshold of reductive glutamine metabolism regulation by HIF-1 | |
| $\lambda_{H,Q_r}$ | 2 | - | Fold change of reductive glutamine metabolism regulation by HIF-1 | |
| $n_{H,Q_r}$ | 4 | - | Hill coefficient | |
| $A_{Q_r}^0$ | 200 | $\mu mol \cdot L^{-1} \cdot s^{-1}$ | Threshold of reductive glutamine metabolism regulation by AMPK | |
| $\lambda_{A,Q_r}$ | 0.5 | - | Fold change of reductive glutamine metabolism regulation by AMPK | |
| $n_{A,Q_r}$ | 2 | - | Hill coefficient | |
| $\underline{A_{Q_?}^0}$ | 250 | $\mu mol \cdot L^{-1} \cdot s^{-1}$ | Threshold for AMPK regulation of GSH | |
| $\underline{\lambda_{A,Q_?}}$ | 5 | - | Fold change of glutathione synthesis regulation by AMPK | |
| $\underline{n_{A,Q_?}}$ | 4 | - | Hill coefficient | |
| $\underline{H_{F_r}^0}$ | 200 | $\mu mol \cdot L^{-1} \cdot s^{-1}$ | Threshold for HIF-1 regulation of reductive fatty acid metabolism. | |

| | | | | |
|---|---|---|---|---|
| $\lambda_{H,F_r}$ | 2 | - | Fold change of reductive fatty acid regulation by HIF-1 | |
| $n_{H,F_r}$ | 4 | - | Hill coefficient | |
| | 29 | | ATP production from glucose oxidation | (8) |
| | 2 | | ATP production from Glycolysis | (9) |
| | 24 | | ATP production from glutamine oxidation | (10,11) |
| | 106 | | ATP production from fatty acid oxidation | (12) |
| | 7 | | ATP consumption in reductive fatty acid metabolism | (12) |
| | 13 | | ATP consumption in reductive glutamine | (13) |
| | 2 | | ATP consumption for GSH synthesis | (14) |

**Supplementary Table 2: Genes selected to evaluate metabolic pathway activity.**
List of genes selected in this study for various metabolic pathways. Gene sets were generated using Gene Ontology database AmiGO (AmiGO 2 version: 2.5.17, (15)). Genes present in multiple pathways were excluded according to a priority list based on the order of appearance in the table.

| Pathway | | Genes used for the scoring metric |
|---|---|---|
| **Catabolic** | AMPK (5) | ACADL, ACADM, ACOX1, ACOX3, ACSL1, ACSL3, ACSL4, ACSL5, ANGPTL4, APOC3, APOE, ATF4, ATF5, BAX, BCL2L11, BTG2, CAT, CCND1, CCND2, CLU, CPT1A, CPT1B, CPT2, CREM, CYP27A1, CYP4A11, CYP7A1, DDB1, DGAT1, DNMT1, EGR1, EHHADH, ELN, FADS2, FASLG, FOS, FOSB, FOSL1, FOXA2, G6PC, G6PC2, G6PC3, GADD45A, GADD45B, GADD45G, GK, HES1, HNF4A, HSPD1, ID1, ID3, JUNB, JUND, KLF5, LPL, MAFA, MAPK9, MECR, MMP9, NCOA2, NR1H3, NR4A1, NR4A2, NUP155, NUP88, NUP98, OLR1, ONECUT1, ONECUT2, PCK1, PCK2, PDK4, PDX1, PRMT1, PRMT3, RUVBL1, SCD, SLC2A4, SOD2, SORBS1, SP1, STAT5A, TOB1, TXNIP. |
| | FAO (F1) (16) | CD36, ACSL1, SLC25A20, CPT1, CPT2, ACADVL, ACADL, ACADM, ACADS, ACADSB, ACAD8, ACAD9, ACAD10, ECHS1, HADH, ACAA1, ACAA2 |
| | Reductive glutamine (Qre) | GLUD2, QARS1, GCLC, CPS1, GCLM, EPRS1, CAD, GLUL, ABAT, GAD2, GAD1, PPAT, ASNS, GFPT1 |
| | Glucose Oxidation (G1) (16) | PDHA1, ACO2, IDH1, OGDH, SDHA, SDHC, FH, MDH1, CS, PC |
| | Mitochondrial ROS (Rm) | NDUFS1, CYTB, SDHA, MAOB, CYCS, VDAC, UCP2, SOD2, CAT, GPX1 |
| | Glutamine oxidation (Q1) | GLS, GLS2, GOT1, GOT2, GLUD1, GPT2 |
| **Anabolic** | HIF-1 (5) | ADM, ALDH4A1, ALDOA, ALDOC, ARHGEF1, ASPH, BHLHE40, BNIP3, BTAF1, CA9, CCNB1, CITED2, CP, DDIT4, EDN1, EGLN1, EGLN3, ENO1, EPRS, ETS1, FN1, GLCCI1, GRK6, HACD3, HSP90B1, IVNS1ABP, KDM3A, MECOM, MET, MXD1, MYLK, NAMPT, NDRG1, NOS2, NOS3, P4HA1, P4HA2, P4HTM, PDGFA, PFKL, PGAM1, PGK1, PLOD1, RARA, RBPJ, RNF165, RRAGD, RSBN1, SERPINE1, SLC31A1, SLC7A6, SOX6, SSRP1, STC2, TFRC, TGFB3, TMEFF1, TMEM45A, VEGFA. |
| | GSH synthesis (QSH) | GGT1, GGT7, GGT5, GSS, OPLAH, CNDP2, GGCT, GGT6 |
| | Reductive glucose (Gre) | G6PC2, G6PC3, G6PC1, PCK2, PCK1, PC, GPI, TPI1, FBP1, FBP2 |
| | Glycolysis (G2) (16) | HK1, GPI, PFKM, ALDOA, TPI1, GAPDH, PGK1, PGAM2, ENO1, PKM |
| | Reductive Fatty acids (Fre) | PCCB, DEGS1, MECR, SCD, PLA2G1B, ABHD3, ACACB, ACSF3, PRKAA2, PTGS2, PTGES, FA2H, FAAH, GSTM4, CYP1A1, MGLL, HTD2, HSD17B8, AKR1C3, FASN, LIPE, ABCD1, PRKAG2, CBR4, ELOVL6, ACACA, MCAT, DECR2, PECR, HPGDS, FADS1, PRKAB2, CBR1, PRXL2B, ACLY, NDUFAB1, PLA2G10, OLAH, ALOX12B, FADS2, ALOX5, LTC4S, ALOX12, ELOVL2, ALOX15B, ELOVL7, PTGDS, PLA2G4A, ALOXE3, ALOX15, TBXAS1, SCD5, PTGS1 |
| | NADPH oxidase-derived ROS (Rn) | CYBB, CYBA, NCF1, NCF2, NCF4, NOX1, NOX3, NOX4, NOX5 |
| **Uptake** | Glucose Uptake (G0) | SLC5A1, SLC5A3, SLC2A7, SLC2A10, SLC2A14, SLC2A6, SLC2A9, SLC2A4, SLC2A8, SLC2A3, SLC2A2, SLC2A1, SLC5A2, SLC2A5 |
| | Fatty Acid Uptake (F0) | SLC27A5, SLC27A1, SLC27A6, SLC27A4, SLC27A2, CD36, FABP3, ABCD1, ABCD2, ABCD3, ABCD4, APOA1, APOA4, APOA5, PLTP, CETP, MTTP, SCARB1, SPNS1, MFSD2A, PITPNB, PITPNM3, PLSCR1, GLTPD2, GLTP |
| | Glutamine Uptake (Q0) | SLC25A22, SLC38A5, SLC6A19, SLC7A5, SLC38A2, SLC38A1, SLC25A13, SLC1A5, SLC38A3, SLC38A8, SLC7A7, SLC7A6, SLC6A14, SLC7A11, SLC38A7 |
| **Oncogene** | MYC | MTDH, ACTL6A, ENO1, BAX, BCAT1, COMMD3-BMI1, POLR3D, CAD, CDC25A, CDK4, CCNB1, CCND2, DDX18, DKC1, E2F3, EIF2S1, EIF4A1, EIF4E, EIF4G1, FOSL1, GAPDH, KAT2A, SLC2A1, GPAM, HUWE1, HMGA1, HSPD1, HSPA4, HSP90AA1, ID2, IREB2, CDCA7, KIR3DL1, LDHA, LIN28B, MAX, NDUFAF2, RIOX2, MMP9, MTA1, MYC, MYCT1, NBN, NME1, NME1-NME2, PMAIP1, NPM1, NCL, ODC1, TP53, PDCD10, PEG10, PFKM, PIM1, PRDX3, PTMA, RCC1, RPL11, SERPINI1, SHMT1, SMAD3, SMAD4, SNAI1, SUPT3H, SUPT7L, BIRC5, TAF10, TAF12, TAF4B, TAF9, TERT, TFRC, RUVBL1, RUVBL2, KAT5, TK1, TRRAP, UBTF |

211

## References:


1. Terunuma A, Putluri N, Mishra P, Mathé EA, Dorsey TH, Yi M, et al. MYC-driven accumulation of 2-hydroxyglutarate is associated with breast cancer prognosis. J Clin Invest. American Society for Clinical Investigation; 2014;124:398–412. Available from: http://dx.doi.org/10.1172/JCI71180

2. Antunes F, Cadenas E. Estimation of H2O2 gradients across biomembranes. FEBS Lett. Wiley; 2000;475:121–6. Available from: http://dx.doi.org/10.1016/s0014-5793(00)01638-0

3. Qutub AA, Popel AS. Reactive oxygen species regulate hypoxia-inducible factor 1alpha differentially in cancer and ischemia. Mol Cell Biol. Informa UK Limited; 2008;28:5106–19. Available from: https://pmc.ncbi.nlm.nih.gov/articles/PMC2519710/

4. Hou X, Song J, Li X-N, Zhang L, Wang X, Chen L, et al. Metformin reduces intracellular reactive oxygen species levels by upregulating expression of the antioxidant thioredoxin via the AMPK-FOXO3 pathway. Biochem Biophys Res Commun. Elsevier BV; 2010;396:199–205. Available from: http://dx.doi.org/10.1016/j.bbrc.2010.04.017

5. Yu L, Lu M, Jia D, Ma J, Ben-Jacob E, Levine H, et al. Modeling the genetic regulation of cancer metabolism: Interplay between glycolysis and oxidative phosphorylation. Cancer Res. 2017;77:1564–74. Available from: http://dx.doi.org/10.1158/0008-5472.CAN-16-2074

6. Zmijewski JW, Banerjee S, Bae H, Friggeri A, Lazarowski ER, Abraham E. Exposure to hydrogen peroxide induces oxidation and activation of AMP-activated protein kinase. J Biol Chem. Elsevier BV; 2010;285:33154–64. Available from: http://dx.doi.org/10.1074/jbc.M110.143685

7. Chua YL, Dufour E, Dassa EP, Rustin P, Jacobs HT, Taylor CT, et al. Stabilization of hypoxia-inducible factor-1alpha protein in hypoxia occurs independently of mitochondrial reactive oxygen species production. J Biol Chem. Elsevier BV; 2010;285:31277–84. Available from: https://pmc.ncbi.nlm.nih.gov/articles/PMC2951202/

8. Flurkey WH. Yield of ATP molecules per glucose molecule. J Chem Educ. American Chemical Society (ACS); 2010;87:271–271. Available from: https://pubs.acs.org/doi/10.1021/ed800102g

9. Berg, J.M., Tymoczko, J.L. and Stryer, L. (2002) Biochemistry. 5th Edition. W. H. Freeman Publishing, New York. - References - Scientific Research Publishing. Available from: https://www.scirp.org/reference/referencespapers?referenceid=807284

10. DeBerardinis RJ, Cheng T. Q's next: the diverse functions of glutamine in metabolism, cell biology and cancer. Oncogene. Springer Science and Business Media LLC; 2010;29:313–24. Available from: https://www.nature.com/articles/onc2009358

11. McKenna MC. Glutamate pays its own way in astrocytes. Front Endocrinol (Lausanne). Frontiers Media SA; 2013;4:191. Available from: https://www.frontiersin.org/journals/endocrinology/articles/10.3389/fendo.2013.00191/full

12. Nelson D, Cox M. Lehninger Biochemie. 3rd ed. Berlin, Germany: Springer; 2005. Available from: http://dx.doi.org/10.1007/978-3-662-08289-8

13. Search BioNumbers - The Database of Useful Biological Numbers. Available from: https://bionumbers.hms.harvard.edu/search.aspx

14. Meister A. Glutathione metabolism and its selective modification. J Biol Chem. Elsevier BV; 1988;263:17205–8. Available from: https://pubmed.ncbi.nlm.nih.gov/3053703/

15. Carbon S, Ireland A, Mungall CJ, Shu S, Marshall B, Lewis S, et al. AmiGO: online access to ontology and annotation data. Bioinformatics. Oxford University Press (OUP); 2009;25:288–9. Available from: https://pubmed.ncbi.nlm.nih.gov/19033274/

16. Jia D, Lu M, Jung KH, Park JH, Yu L, Onuchic JN, et al. Elucidating cancer metabolic plasticity by coupling gene regulation with metabolic pathways. Proc Natl Acad Sci U S A. Proceedings of the National Academy of Sciences; 2019;116:3909–18. Available from: http://dx.doi.org/10.1073/pnas.1816391116